Comments on Inorganic Chemistry
Publication details, including instructions for authors and subscription information:
http://www.informaworld.com/smpp/title~content=t713455155

Metallocryptands: Host Complexes for Probing Closed-Shell Metal-Metal Interactions

Vincent J. Catalano; Byron L. Bennett; Mark A. Malwitz; Renante L. Yson; Heidi M. Kar; Stamatis Muratidis; Stephen J. Horner

Online publication date: 24 June 2010

To cite this Article Catalano, Vincent J. , Bennett, Byron L. , Malwitz, Mark A. , Yson, Renante L. , Kar, Heidi M. , Muratidis, Stamatis and Horner, Stephen J.(2003) 'Metallocryptands: Host Complexes for Probing Closed-Shell Metal-Metal Interactions', Comments on Inorganic Chemistry, 24: 1, 39 — 68
To link to this Article: DOI: 10.1080/02603590390237236
URL: http://dx.doi.org/10.1080/02603590390237236

Comments on Inorganic Chemistry, 24: 39–68, 2003

ISSN: 0260-3594 print
DOI: 10.1080/02603590390237236

Taylor & Francis
Taylor & Francis Group

Metallocryptands: Host Complexes for Probing Closed-Shell Metal-Metal Interactions

Vincent J. Catalano*, Byron L. Bennett, Mark A. Malwitz, Renante L. Yson, Heidi M. Kar, Stamatis Muratidis and Stephen J. Horner
Department of Chemistry, University of Nevada, Reno
Reno, NV 89557, USA

Metallocryptands are inorganic host complexes that contain a central metal ion, around which are arranged three multi-dentate ligands capped by a trigonally coordinated d^{10} transition metal (Pt(0), Pd(0), and Au(1)). These very large cage complexes are capable of incarcerating a variety of metals, metal ions and anions including alkali metal ions, Hg_2^{2+}, Hg^0, Tl^+, Pb^{2+} and with modification the halides. Many of the metal-metal interactions within these complexes are shorter than the sum of the respective covalent radii often resulting in complexes that are highly luminescent.

Keywords: metallocryptands, metal-metal interactions, encapsulation, cage, liminescence

INTRODUCTION

There has been a resurgence of interest in the attractive interactions between closed-shell heavy metal atoms and ions. Numerous examples of heavy metal ions such as Au(I), Ag(I), Tl(I) or Pb(II), or metal atoms such as Pt(0), Pd(0), Hg(0), associating with each other or with other like-species are found in the literature.[1,2] Elucidating the nature of these attractive interactions has been the subject of considerable theoretical effort. The role of dispersion forces as the primary attractive force in metallophilic attractions has only recently been clarified,[3] whereas relativistic effects may also play a significant role in maintaining the attraction between Au(I) centers.[4]

*E-mail: vjc@unr.edu

The strength of these interactions is on the order of H-bonds, and often these aggregates dissociate into their monomeric components in solution. For example, Crespo et al.[5] reported an unsupported Au(I)-Tl(I) linear chain compound with metal-metal separations just over 3.0 Å. This yellow solid is highly luminescent in the solid state but dissociates in solution to produce a colorless, non-luminescent 1:1 electrolyte. Previously, Fackler and coworkers[6] employed the anionic MTP ($CH_2P(S)Ph_2$) ligand to form extended one-dimensional chains of Au-Tl or Au-Pb-Au with metal-metal separations just under 3.0 Å. Interestingly, the Pb-containing species is luminescent at room temperature in fluid solution while the Tl-containing species is not. Similarly, the polymeric $\{Tl[Au(C_6Cl_5)_2]\}_n$ complex is intensely luminescent in the solid state, and exposure to solvent vapor significantly perturbs the emission, enabling this material to be used as a vapochromic sensor.[7] These interactions are not limited to linear, one-dimensional chains, and a number of interesting complexes containing cyclic, trinuclear Au(I) subunits sandwiching other metal ions have recently been reported. Like their linear counterparts, these multimetallic array are not particularly stable in solution; however, the solids are luminescent.[8]

In order to more effectively probe metal-metal interactions in solution, we have employed a cage approach where a guest metal atom or ion is effectively incarcerated into the center of a metallocryptand cage as denoted in Scheme 1. For the most part, these cages are static binders of metal ions, allowing the guest-capping metal interactions to be easily probed in solution and in the solid state. Previously established nomenclature uses the term

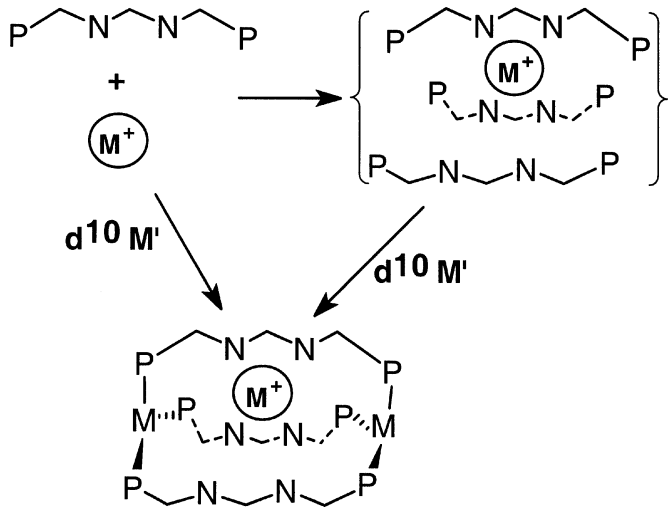

SCHEME 1

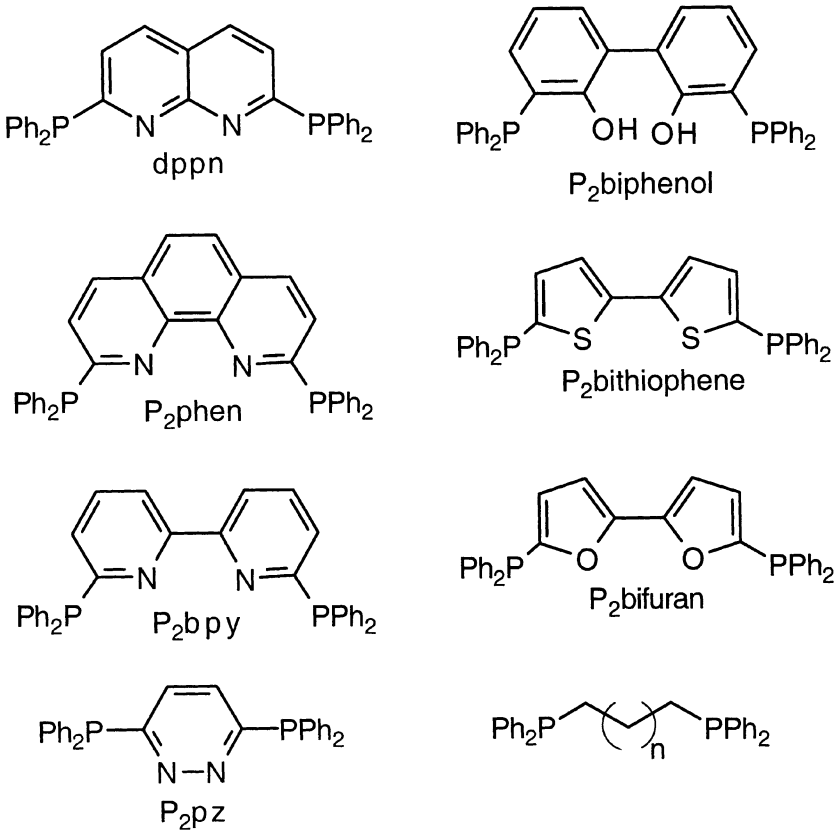

CHART 1

"metallocryptand" to describe the empty cage complex while "metallocryptate" is used to describe the complex that contains an encapsulated metal ion.

There are several factors influencing metallocryptate formation, and many of these are related to the multidentate ligand. Chart 1 presents the ligands that are effective for cage formation (left column) along with several variations that have not produced cage complexes (right column) in our laboratory. Each of these ligands contains soft, outer Lewis bases (diphenylphosphine groups) along with harder internal Lewis donor atoms, using imine groups. These air-stable ligands are easily synthesized in high yield by either reaction of the dihalo-precursor with lithium diphenylphosphide or by direct lithiation of the ligand precursor followed by quenching with chlorodiphenylphosphine.

As shown in Scheme 1, the metalation reactions producing the metallocryptate can follow either a template mechanism, where the guest metal ion is first stabilized through coordination to the internal donor groups of the multidentate ligand followed by addition of the appropriate d^{10}-containing capping metal starting material, or by a "self-assembly" reaction where all of the components are added in a single step. Surprisingly, this simple second method has been the most successful. Polymer formation, common in multidentate coordination chemistry, thus far has only been observed with the 3,6-bis(diphenylphosphino)pyridazine (P_2pz) ligand.

Closed-shell d^{10} metals are chosen as capping groups for several reasons. Primarily, d^{10} metals are known to adopt the necessary three-coordinate trigonal planar geometry required for metallocryptand formation, but also because their filled d_{z^2} and empty p_z orbitals are properly oriented to overlap with the guest metal ion. Additionally, trigonally coordinated d^{10} metal complexes are known to be highly luminescent with this emission originating from a $d \rightarrow p_z$ transition. Perturbation of this p_z orbital by guest metal encapsulation could form the basis of a luminescent sensor for metal ions.

This notion was first tested using 2,9-bis(diphenylphosphino)-1, 8-naphthyridine, dppn.[9] According to Scheme 2, the pale-yellow, sodium-containing metallocryptate, $[Au_2Na(\mu\text{-dppn})_3](PF_6)_3$, **1**,[10] is easily synthesized by reaction of three equivalents of dppn with two equivalents of Me_2SAuCl in acetonitrile followed by addition of excess $NaPF_6$. As shown by $^{31}P\{^1H\}$ NMR spectroscopy the sodium ion acts as a template, organizing the dppn ligands prior to addition of the Au centers. In CD_3CN the free dppn ligand shows a single resonance at 0.7 ppm. Addition of $NaPF_6$ generates bright orange solution with broad resonances for the dppn ligand at 2.0 and 3.3 ppm and a signal for the PF_6^- anion. Addition of Me_2SAuCl to this solution produces a yellow solution with a new resonance at 43 ppm attributed to the metallocryptate. The order of addition may be reversed, indicating that the empty metallocryptand can be formed first, followed by partition of the sodium ion into the cavity.

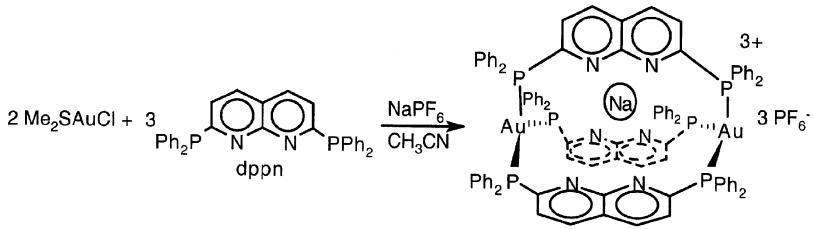

1

SCHEME 2

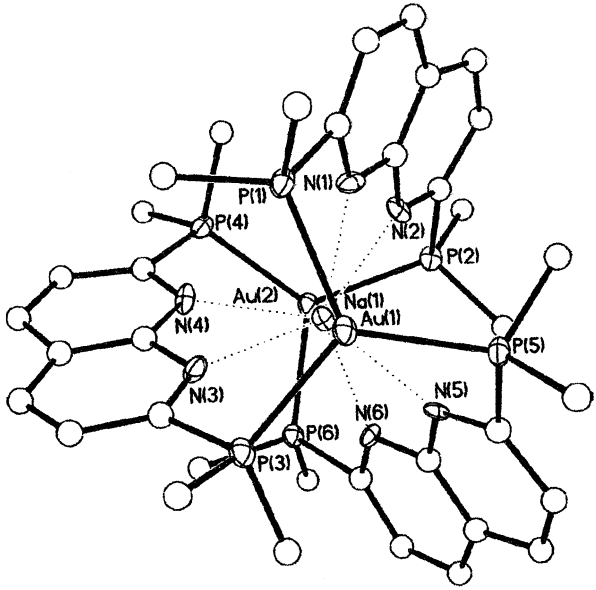

FIGURE 1 X-ray structural diagram for cation of $[Au_2Na(\mu\text{-dppn})_3](PF_6)_3$, **1**, with hydrogen atoms and all but the ispo carbons of the phenyl rings removed for clarity. Carbon atoms are denoted with open circles. Selected bond distances (Å): Au(1)–Na(1) 3.544(6), Au(2)–Na(1) 3.584(6), Au(1)–P(1) 2.368(4), Au(2)–P(2) 2.372(4), Au(1)–P(3) 2.371(4), Au(2)–P(4) 2.376(4), Au(1)–P(5) 2.370(4), Au(2)–P(6) 2.386(4), Na(1)–N(1) 2.462(12), Na(1)–N(4) 2.470(12), Na(1)–N(2) 2.446(12), Na(1)–N(5) 2.484(12), Na(1)–N(3) 2.467(13), Na(1)–N(6) 2.458(12), Au(1)···Au(2) 7.126(2). Angles (°): Au(1)–Na(1)–Au(2) 178.5(2), P(2)–Au(1)–P(4) 122.24(13), P(1)–Au(1)–P(3) 116.99(14), P(2)–Au(1)–P(6) 116.73(13), P(1)–Au(1)–P(5) 120.30(14), P(4)–Au(1)–P(6) 118.56(14), P(3)–Au(1)–P(5) 120.77(14), P(1)–Au(1)–Au(2)–P(2) 92.1(1), P(1)–Au(1)–Au(2)–P(4) 31.0(1), P(3)–Au(1)–Au(2)–P(4) 86.5(1), P(2)–Au(1)–Au(2)–P(5) 28.9(1), P(5)–Au(1)–Au(2)–P(6) 88.6(1), P(3)–Au(1)–Au(2)–P(6) 32.8(1).

The X-ray crystal structure of **1** is presented in Figure 1. The structure contains two trigonal Au(I) centers coordinated to the phosphine portions of the dppn ligands. The sodium ion sits in the center of the D_3 symmetric cavity formed by the naphthyridine ligands with long, non-bonding Na(1)-Au(1) and Na(1)-Au(2) separations of 3.544(6) and 3.584(6) Å, respectively. These molecules and all the metallocryptands reported here are helical; however, as dictated by the centrosymmetric space groups, they are racemic. The Na^+ ion is tightly held by the imine moieties exhibiting an average Na-N distance of 2.46 Å. It is these short Na-N separations that are responsible for

maintaining this three-metal assembly in the solution state and turning off ligand substitution at the Au(I) centers. In the solid state **1** is strongly emissive with a long-lived (280 μs) low energy band (566 nm, $\lambda_{exi} =$ 355 nm). This emission is significantly quenched in solution, presumably by solvent coordination to the trigonal AuP_3 face, and only a fluorescence associated with an intraligand band is observed. Substitution of sodium ion for other alkali metals does not significantly alter the emission properties, suggesting that the metallocryptand cage based on the dppn ligand is not an effective luminescent probe of alkali metal. This may result from the limited interaction between the capping Au(I) ions and the internal metal ion.

To explore this idea we prepared the analogous compound using 2,9-bis-(diphenylphosphino)-1,10-phenanthroline (P_2phen).[9] Although both dppn and P_2phen have similar donor properties, the P_2phen ligand has a shorter $P \cdots P$ separation (~ 7.0 vs. 7.5 Å) which should enable a shorter metal-metal interaction in the resulting P_2phen-based metallocryptate. Additionally, because of the curvature of the phenanthroline portion of the ligand compared to the linear arrangement in dppn, the internal cavity of a P_2phen based-metallocryptate should be larger than the corresponding dppn-metallocryptate giving the encapsulated ion a greater degree of freedom.

Similar to the formation of **1**, the reaction of tetrahydrothiophenegold(I) chloride ((tht)AuCl) with P_2phen and excess $NaPF_6$ produces yellow $[Au_2Na(P_2phen)_3](PF_6)_3$, **2**,[11] as shown in Scheme 3. In solution the encapsulation of Na^+ ion is dynamic, and an equilibrium is established between the metallocryptate, empty metallocryptand and the empty metallomacrocycle formed upon dissociation of one P_2phen ligand, according to Equations 1 and 2. The equilibrium constants were measured by $^{31}P\{^1H\}$ NMR spectroscopy ($K_1 \approx 5$, $K_2 \approx 1.6 \times 10^{-4}$, chlorocarbon) indicating that the empty

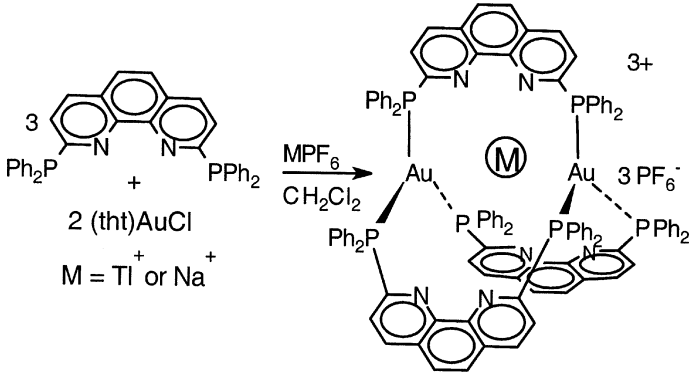

SCHEME 3

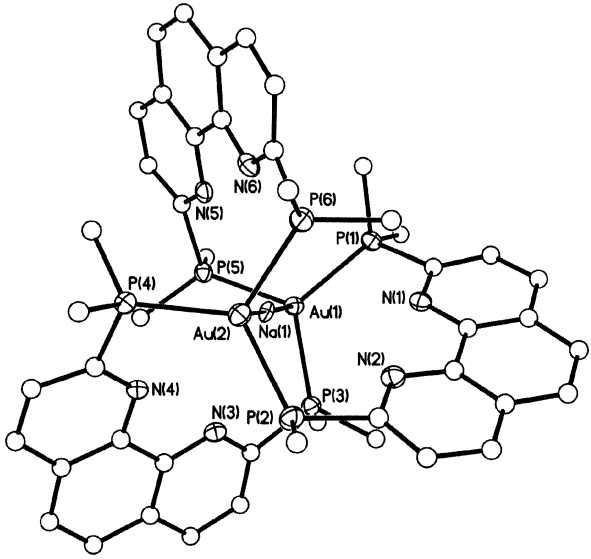

FIGURE 2 Structural diagram of cationic portion of $[Au_2Na(\mu\text{-}P_2phen)_3](PF_6)_3$, **2**, with hydrogen atoms and all but the ispo carbons of the phenyl rings removed for clarity. Carbon atoms are drawn as open circles. Selected bond lengths (Å) and angles (°) for **2**: Au(1)–Na(1) 2.797(13), Au(2)–Na(1) 2.813(13), Na(1)–N(1) 3.471(7), Na(1)–N(2) 3.427(7), Na(1)–N(3) 3.260(7), Na(1)–N(4) 3.294(7), Na(1)–N(5) 3.343(7). Na(1)–N(6) 3.368(7), Au(1)–P(1) 2.3701(16), Au(1)–P(3) 2.3685(16), Au(1)–P(5) 2.3662(15), Au(2)–P(2) 2.3615(16), Au(2)–P(4) 2.3627(16), Au(2)–P(6) 2.3716(17)Å, Au(1)–Na(1)–Au(2) 177.4(6), Au(1)–Na(1)–Au(2) 157.2(5), P(1)–Au(1)–P(3) 120.27(6), P(1)–Au(1)–P(5) 119.37(6), P(3)–Au(1)–P(5) 117.57(6), P(2)–Au(2)–P(4) 123.17(6), P(4)–Au(2)–P(6) 116.06(6), P(2)–Au(2)–P(6) 117.78(6), P(1)–Au(1)–Au(2)–P(2) 101.7(1), P(3)–Au(1)–Au(2)–P(4) 104.9(1), P(5)–Au(1)–Au(2)–P(6) 105.3(1)°.

$$[Au_2Na(P_2phen)_3](PF_6)_3 \overset{K_1}{\rightleftharpoons} [Au_2(P_2phen)_3](PF_6)_2 + NaPF_6 \qquad (1)$$

$$[Au_2(P_2phen)_3](PF_6)_2 \overset{K_2}{\rightleftharpoons} [Au_2(P_2phen)_2](PF_6)_2 + P_2phen \qquad (2)$$

metallocryptand is the predominant species in solution. However, addition of excess sodium ion drives the equilibrium towards **2**, and X-ray quality crystals can be isolated upon slow diffusion of diethyl ether. Figure 2 presents an X-ray structural drawing of the cation of **2**. Like **1** it contains a central sodium ion in a D_3 symmetric cage formed by the three P_2phen ligands. However, unlike **1**, the sodium ion of **2** strongly interacts with the Au(I)

capping metals with Au(1)-Na(1) and Au(2)-Na(1) separations of 2.797(13) and 2.813(13) Å, respectively. The electrostatic repulsion between the Au(I) centers and the cationic Na^+ ion, along with the lack of stabilization by the imine nitrogen atoms of the P_2phen ligands, produce a very weakly bound guest metal, explaining the equilibrium observed in solution.

Addition of Tl^+ ion to this equilibrium mixture produces a single species that is not dynamic and exhibits a single resonance at 45.7 ppm in the $^{31}P\{^1H\}$ NMR spectrum with coupling to Tl ($^2J_{P\text{-}Tl} = 186$ Hz, ^{203}Tl 29.5% abundant, $I = 1/2$; ^{205}Tl 70.5% abundant, $I = 1/2$). Because of the large linewidths and nearly identical gyromagnetic ratios, the individual couplings to ^{203}Tl and ^{205}Tl could not be differentiated. Additionally, the presence of Tl is

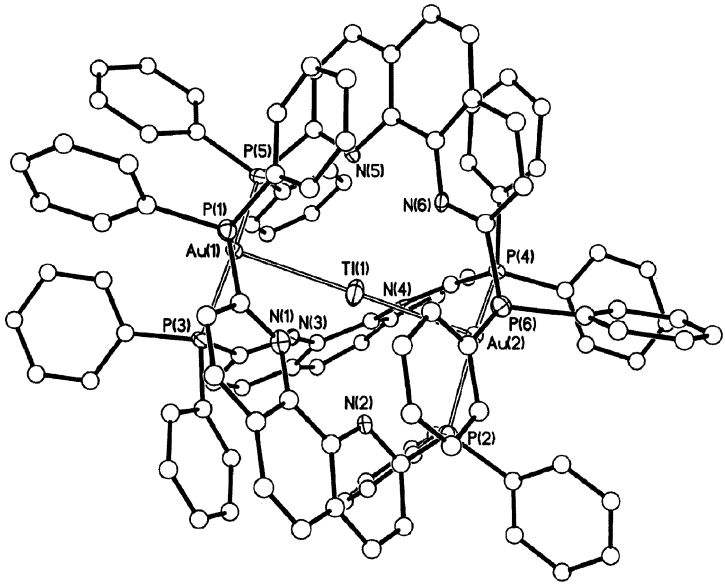

FIGURE 3 Thermal ellipsoid plot (40% probability) of the cation of $[Au_2Tl(P_2\text{-}phen)_3](PF_6)_3$, **3** with phenyl rings shown to emphasize their axial and equatorial orientation. Hydrogen atoms omitted for clarity and carbon atoms drawn as open circles. Selected bond lengths (Å) and angles (°) for **1**: Au(1)–Tl(1) 2.9171(5), Au(2)–Tl(1) 2.9109(5), Tl(1)–N(1) 3.178(5), Tl(1)–N(2) 3.208(5), Tl(1)–N(3) 3.321(5), Tl(1)–N(4) 3.193(5), Tl(1)–N(5) 3.329(5), Tl–N(6) 3.158(5), Au(1)–P(1) 2.388(3), Au(1)–P(3) 2.381(2), Au(1)–P(5) 2.380(2), Au(2)–P(2) 2.368(2), Au(2)–P(4) 2.377(2), Au(2)–P(6) 2.381(3)Å, Au(1)–Tl(1)–Au(2) 174.47(2), P(1)–Au(1)–P(3) 120.15(8), P(1)–Au(1)–P(5) 118.15(8), P(3)–Au(1)–P(5) 120.18(8), P(2)–Au(2)–P(4) 123.77(8), P(4)–Au(2)–P(6) 118.07(8), P(2)–Au(2)–P(6) 116.68(8), P(1)–Au(1)–Au(2)–P(2) 107.1(1), P(3)–Au(1)–Au(2)–P(4) 110.9(1), P(5)–Au(1)–Au(2)–P(6) 109.0(1)°.

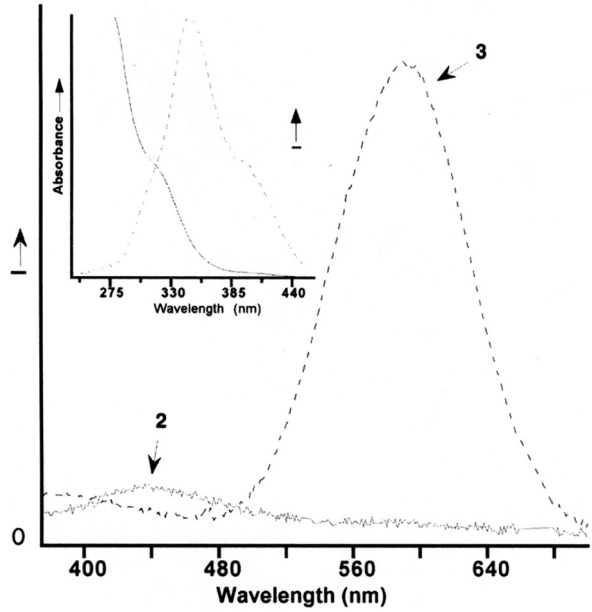

FIGURE 4 Emission spectra of $[Au_2Tl(P_2Phen)_3](PF_6)_3$, **3** (dashed line) and of $[Au_2Na(\mu\text{-}P_2phen)_3](PF_6)_3$, **2** (solid line) in acetonitrile with $\lambda_{exi} = 340$ nm. Inset: Electronic absorption (solid line) and excitation (dashed line, $\lambda_{mon} = 590$ nm) spectra of **3** (CH_3CN).

confirmed by the observation of a septet (δ 749.9 ppm, $^2J_{P\text{-}Tl} = 186$ Hz) in the ^{205}Tl NMR spectrum, indicating a single ^{205}Tl environment coupled to six chemically equivalent phosphorus atoms. This formulation is further supported in the solid state where crystals of $[Au_2Tl(\mu\text{-}P_2phen)_3](PF_6)_3$, **3**,[11] are easily isolated from the above solution.

The X-ray crystal structure (Fig. 3) is very similar to **2** except the center of the metallocryptand cage is occupied by a single Tl cation with short Au-Tl separations of 2.9171(5) and 2.9109(5) Å. Likewise, the Tl-N distances (ave. 3.23 Å) are long, indicating that the Au-Tl interactions are the predominant attractive forces holding the Tl(I) ion in this cage, in marked contrast to **1** where ligand guest interactions are responsible for maintaining the assembly.

Like many other compounds that contain Au(I)-Tl(I) interactions, **3** is intensely emissive in solution and in the solid state (Fig. 4). In solution a strong (solvent independent) emission is observed at 600 nm that originates from what appears to be a metal-covered transition (420 nm). The long lifetime of this emission in the solution state (10 μs) and solid state (220 μs) may be attributed to the protection afforded by the phenyl rings of the P_2phen

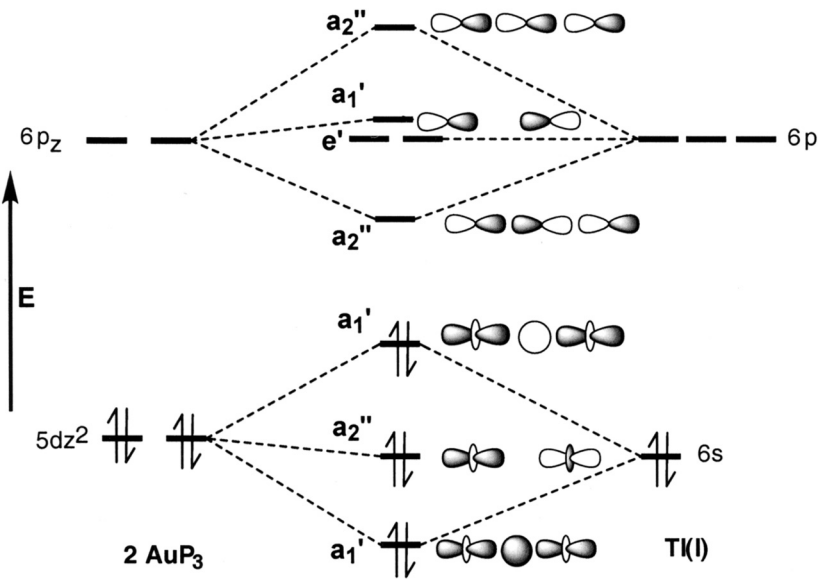

FIGURE 5 Simplified molecular orbital diagram ignoring metal-metal π-bonding depicting the interaction between two trigonally coordinated d^{10} metal ions with the filled s and empty p orbitals on a Tl^{+} ion in the D_{3h} point group.

ligands to the Au-Tl-Au chromophore. As seen in Figure 3, these phenyl rings adopt two orientations, axial and equatorial, effectively blocking access to the AuP_3 face by solvent or other small molecules like oxygen. The emission of **3** is insensitive to molecular oxygen.

We have proposed a simple qualitative molecular orbital picture (Figure 5) similar to that proposed by Balch and coworkers[12] to explain the strong Au-Tl interactions observed in **3**. Although formally non-bonding, interaction between the filled Au $5d_{z^2}$, empty Au $6p_z$, Tl 6s and Tl $6p_z$ orbitals produces a set of metal-metal sigma bonding, nonbonding and anti-bonding orbitals. Mixing between levels stabilizes the filled orbitals relative to their virtual counterparts, leading to an attractive interaction between these metals.

Assuming that this M.O. picture is correct, other metals isoelectronic with Au(I) would also exhibit a similar stabilization with Tl(I). Zero valent Pt and Pd are two such metals known to form trigonally coordinated phosphine complexes. Addition of $TlNO_3$ to a dichloromethane solution of either $Pt(dba)_2$ or $Pd_2(dba)_3{\cdot}CHCl_3$ (dba is dibenzylideneacetone) and the P_2phen ligand produces deep-red, air-stable complexes identified as $[Pd_2Tl(P_2phen)_3](NO_3)$, **4**, and $[Pt_2Tl(P_2phen)_3](NO_3)$, **5**.[13] It is interesting to note that complex formation occurs before oxidative addition of solvent; however, both **4**

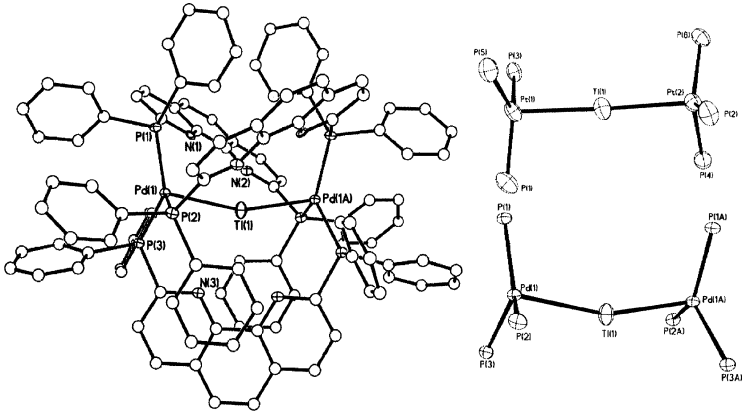

FIGURE 6 X-ray structural drawing of cationic portion of $[Pd_2Tl(P_2phen)_3](NO_3)$, **4**, (left) cores and $[Pt_2Tl(P_2phen)_3](NO_3)$, **5** (top right) and **4** (bottom right). Selected bond distances (Å) and angles (°) for **4**: Pd(1)–Tl(1) 2.7914(6), Pd(1)···Pd(2) 5.503(2), Pd(1)–P(1) 2.3254(2), Pd(1)–P(2) 2.326(2), Pd(1)–P(3) 2.310(2), Tl(1)–N(1) 3.91(1), Tl(1)–N(2) 3.76(1), Tl(1)–N(3) 3.19(1), Pd(1)-Tl(1)–Pd(2) 160.62(3), P(1)–Pd(1)–P(3) 120.63(7), P(1)–Pd(1)–P(2) 122.40(7), P(3)–Pd(1)–P(2) 110.02(7), P(1)–Pd(1)–Tl(1) 105.51(5), P(2)–Pd(1)–Tl(1) 93.88(5), P(3)–Pd(1)–Tl(1) 96.16(5). **5**: Pt(1)–Tl(1) 2.7907(9), Pt(2)–Tl(1) 2.7919(9), Pt(1)···Pt(2) 5.578(1), Pt(1)–P(1) 2.269(5), Pt(1)–P(3) 2.284(4), Pt(1)–P(5) 2.279(4), Pt(2)–P(2) 2.298(4), Pt(2)–P(4) 2.277(4), Pt(2)–P(6) 2.281(4), Tl(1)–N(1) 3.60(2), Tl(1)–N(2) 3.63(2), Tl(1)–N(3) 3.39(2), Tl(1)–N(4) 3.38(2), Tl(1)–N(5) 3.69(2), Tl(1)–N(6) 3.73(2), Pt(1)–Tl(1)–Pt(2) 175.27(3), P(1)–Pt(1)–P(3) 119.00(16), P(1)–Pt(1)–P(5) 124.50(16), P(3)–Pt(1)–P(5) 111.40(16), P(2)–Pt(2)–P(4) 114.42(18), P(4)–Pt(2)–P(6) 119.97(17), P(2)–Pt(2)–P(6) 119.43(16), P(1)–Pt(1)–Pt(1)–Tl(1) 97.90(13), P(3)–Pt(1)–Tl(1) 95.84(11), P(5)–Pt(1)–Tl(1) 98.67(11), P(2)–Pt(2)–Tl(1) 97.77(11), P(4)–Pt(2)–Tl(1) 95.99(12), P(6)–Pt(2)–Tl(1) 101.04(11).

and **5** are more effectively produced in the absence of chlorocarbon. As shown in Figure 6, the structures of **4** and **5** are very similar except the Tl atom of **4** resides on a crystallographic two-fold axis. Both contain short M-Tl separations of 2.7914(6) Å for Pd(1)-Tl(I) in **4** and 2.7907(9) and 2.7953(2) Å for Pt(1)-Tl(I) and Pt(2)-Tl(I) in **5**. The M-Tl-M linkage in **4** is considerably more distorted from linearity at 160.62(3)° while in **5** this angle opens to 175.27(3)°.

In solution both **4** and **5** have resonances in the $^{31}P\{^1H\}$ NMR spectrum in the "metallocryptand region" at 27.1 and 46.1 ppm respectively, yet neither complex shows any coupling between the phosphorus atoms on the P_2phen ligand and the encapsulated Tl ion, in marked contrast to the $^2J_{P\text{-}Tl}$ of 186 Hz observed for the isoelectronic and structurally very similar

$[Au_2Tl(P_2phen)_3]^{3+}$ complex. The origin of this is not quite understood but may be related to a diminution of s orbital contribution to the metal-metal interaction in the Pt(0) and Pd(0) systems. Both **4** and **5** possess single resonances in the ^{205}Tl NMR spectrum at $+2022$ and $+1866$ ppm versus external $TlNO_{3(aq)}$, and **5** additionally exhibits coupling to ^{195}Pt with a $^1J_{Tl\text{-}Pt} = 5560$. This coupling is also reproduced in the ^{195}Pt NMR spectrum that shows a doublet of quartets at -4119 ppm vs. $H_2PtCl_{6(aq)}$ confirming coupling to three equivalent ^{31}P nuclei ($^1J_{Pt\text{-}P} = 4436$) and a single Tl nucleus (^{195}Pt 33.8% abundant, $I = 1/2$). Both **4** and **5** have broad and intense low energy absorptions in CH_2Cl_2 at 423 nm ($47000\,M^{-1}\,cm^{-1}$) and 454 nm ($26000\,M^{-1}\,cm^{-1}$). Unlike their Au(I) counterparts no visible emission was observed from either of these solutions.

Also evident from the M.O. picture above is that other s^2 metal ions should have a similar propensity to form metallocryptates. Even though there are several solid state aggregations exhibiting short separations between Pb^{2+} ions and Au(I) centers, the attempted encapsulation of Pb^{2+} into the Au(I)-P_2phen-based metallocryptand failed. This may be a consequence of the high overall cationic charge that would result from sandwiching a dication between two monocations. However, replacing Au(I) center with the zero-valent Pd(0) or Pt(0) metals allows for the facile incorporation of Pb^{2+} ion. The air-stable, deep green/brown $[Pd_2Pb(P_2phen)_3](ClO_4)_2$, **6**, and $[Pt_2Tl(P_2phen)_3](ClO_4)_2$, **7**,[14] are easily produced in ca. 75% yield according to Equations 3 and 4.

$$Pd_2(dba)_3 \cdot CHCl_3 + 3P_2phen + Pb(ClO_4)_2 \rightarrow [Pd_2Pb(P_2phen)_3](ClO_4)_2 + 3dba + CHCl_3 \quad (3)$$

$$2Pt(dba)_2 + 3\ P_2phen + Pb(ClO_4)_2 \rightarrow [Pt_2Pb(P_2phen)_3](ClO_4)_2 + 4dba \quad (4)$$

Like their Tl(I) containing analogs both **6** and **7** have single resonances in the $^{31}P\{^1H\}$ NMR spectra at 29.8 and 48.1 ppm respectively, and like their Tl(I) analogs, coupling to ^{207}Pb(22% abundant, $I = 1/2$) is not observed. Accordingly, the ^{195}Pt NMR spectrum of $[Pt_2Pb(P_2phen)_3](ClO_4)_2$ shows the anticipated quartet ($^1J_{Pt\text{-}P} = 4085$ Hz) at $+2916$ ppm without resolvable $^1J_{Pt\text{-}Pb}$ coupling. The electronic absorption spectrum of **6** shows a low energy band at 481 nm while a similar band at 470 nm is evident for **7**. Neither complex is visibly luminescent.

As determined by X-ray crystallography (Figure 7), both **6** and **7** contain exceptionally short separations between these closed-shell metals. In **6** the Pd(1)-Pb(1) and Pd(2)-Pb(1) separations are nearly identical at 2.7095(6) and 2.6902(6) Å respectively, and the Pb center is nearly linearly bonded with a Pd(1)-Pb(1)-Pd(2) angle of 178.75(1)°, indicating the lone pair is stereochemically inactive. Like the other P_2phen-based systems the

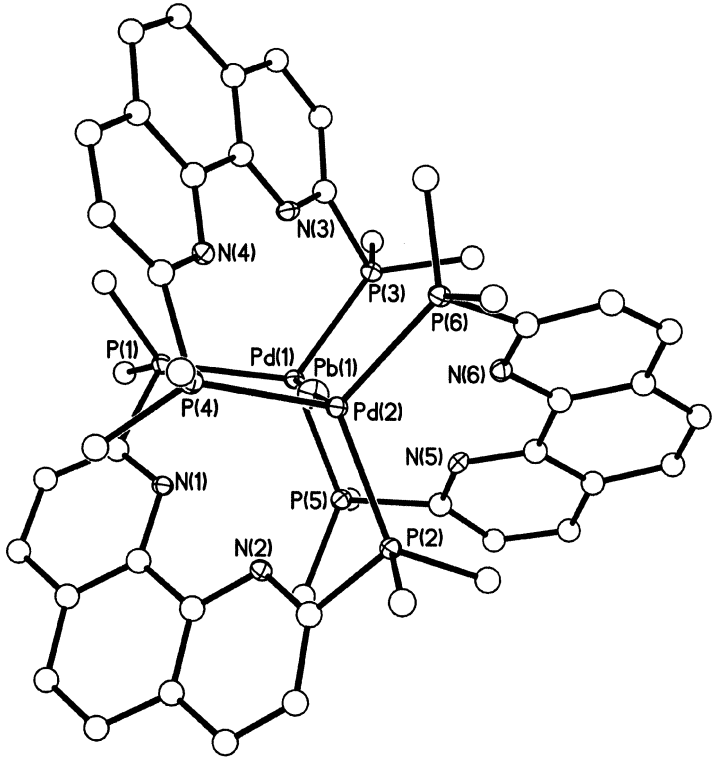

FIGURE 7 Thermal ellipsoid plot (40%) of cationic portion of $[Pd_2Pb(P_2phen)_3](ClO_4)_2$, **6** with carbon atoms drawn as open circles and hydrogen atoms removed for clarity. All but the ipso carbon of the phenyl rings are moved for clarity. Selected distances (Å) and angles(°): Pd(1)–Pb(1) 2.7095(6), Pd(2)–Pb(1) 2.6902(6), Pb(1)–N(1) 3.090(2), Pb(1)–N(2) 3.095(2), Pb(1)–N(3) 3.090(2), Pb(1)–N(4) 3.215(2), Pb(1)–N(5) 3.156(2), Pb(1)–N(6) 3.166(2), Pd(1)–Pb(1)–Pd(2) 178.75(1), P(1)–Pd(1)–P(3) 119.41(5), P(1)–Pd(1)–P(5) 117.27(4), P(3)–Pd(1)–P(5) 121.30(5), P(2)–Pd(2)–P(4) 120.15(4), P(2)–Pd(2)–P(6) 116.42(4), P(4)–Pd(2)–P(6) 120.21(5).

guest-nitrogen separations are long (ave. Pb-N = 3.142(1) Å) and are considered non-bonding. The structure of **7** is nearly identical to **6** with Pt(1)-Pb(1) and Pt(2)-Pb(1) separations of only 2.7469(6) and 2.7325(6) Å. It is noteworthy that these separations are extremely short and are as short or shorter than those formed through insertion reactions producing covalently bonded M-Pb complexes,[15] suggesting that these non-covalent interactions are comparable in strength to legitimate covalent metal-metal bonds.

As a further probe of this idea, it is desirable to determine the "natural" metal-metal separation in these complexes—that is the separation in the absence of any ligand constraints. In all of the P_2phen-based metallocryptands the capping metals are "puckered" inward towards the central metal, suggesting that either they have a very high affinity for each other or that the ligand constrains the d^{10} metal atom into this position. Replacing the P_2phen ligand with P_2bpy introduces an element of flexibility to the ligand backbone while keeping constant the donor properties. It was anticipated that rotation about the carbon-carbon bond connecting the two pyridine rings would allow for easier twisting of the two trigonal planes formed by the MP_3 subunits which, in turn, allows for a shorter metal-metal separation. Similar to **4** and **5** reaction of P_2bpy with the appropriate Pt(0) or Pd(0) starting material in the presence of Tl^+ ion produces $[Pd_2Tl(P_2bpy)_3](NO_3)$, **8**, and $[Pt_2Tl(P_2bpy)_3](NO_3)$, **9**,[13] as deep-red, air stable products. These complexes are isostructural and crystallize in the rhombohedral space group R-3c with only one-sixth of the molecule in the asymmetric unit (Fig. 8). Because of this high symmetry the M-Tl-M angles are rigorously 180°, and the P-M-P angles are equal at ca. 117.5°. In **8** the Pd(1)-Tl(1) separation is 2.7678(6) Å, and in **9** the Pt(1)-Tl(1) distance is 2.7953(2) Å. These separations are nearly identical to those observed in **4** and **5**, indicating ligand rigidity is not a hindrance to forming short metal-metal separations in these metallocryptands. The more relaxed nature of the ligand backbone is

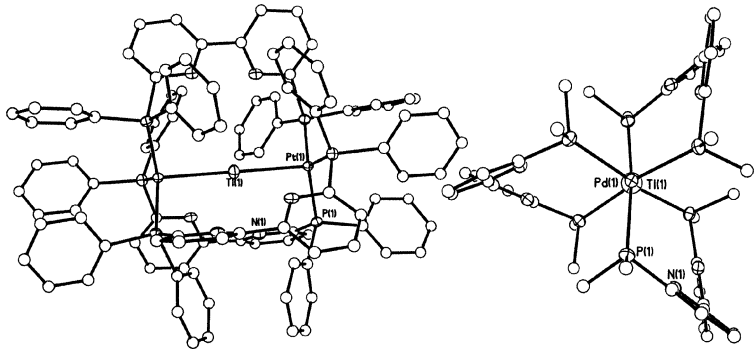

FIGURE 8 X-ray structural drawing of cationic portion of $[Pt_2Tl(P_2bpy)_3](NO_3)$, **9**, (left) with carbon atoms drawn as open circles and hydrogen atoms removed for clarity and $[Pd_2Tl(P_2bpy)_3](NO_3)$, **8** (right, with phenyl rings removed) viewed end-on emphasizing the three-fold symmetry. Selected bond distances (Å) and angles (°) for **9**: Pt(1)–Tl(1) 2.7953(2), Pt(1)···Pt(2) 5.591(1), Pt(1)–P(1) 2.312(1), Tl(1)–N(1) 3.886(5), Pt(1)–Tl(1)–Pt(2) 180, P(1)–Pt(1)–P(3) 117.685(14), P(1)–Pt(1)–Tl(1) 98.83(3). **8**: Pd(1)–Tl(1) 2.7678(6), Pd(1)···Pd(2) 5.536(2), Pd(1)–P(1) 2.345(1), Tl(1)–N(1) 3.89(2), Pd(1)–Tl(1)–Pd(2) 180, P(1)–Pd(1)–P(3) 117.44(2), P(1)–Pd(1)–Tl(1) 99.29(4).

manifested both by the staggered configuration of the two MP_3 planes and in the large dihedral angle between the pyridine rings of the P_2bpy ligands (46°). The rigid phenanthroline group of P_2phen constrains this angle to 0°. In the P_2bpy complexes this arrangement increases the Tl-N separations to ~ 3.9 Å, reinforcing the idea that metallocryptand formation can be achieved without cooperation from the internal donors, though they are needed for synthesis of the ligands. Additionally, the lone pairs on the pyridine rings are not even directed toward the Tl^+ ion.

The successful encapsulation of s^2 heavy metal ions (Tl^+ and Pb^{2+} begs the question of whether other s^2 metals or metal ions could be successfully trapped into the metallocryptand cage. Reactions with Sn^{2+} and In^+ produce unstable products and were not explored further. However, simply stirring an acetonitrile solutions of three equivalents of P_2phen with 2 equivalents of (tht)AuCl and single drop of elemental mercury yields a lemon-yellow solution from which quicksilver-containing $[Au_2Hg(P_2phen)_3](PF_6)_2$, **10**[16] can be isolated by addition of NH_4PF_6 and slow removal of the solvent. The presence of Hg is confirmed by the $^{31}P\{^1H\}$ NMR spectroscopy,

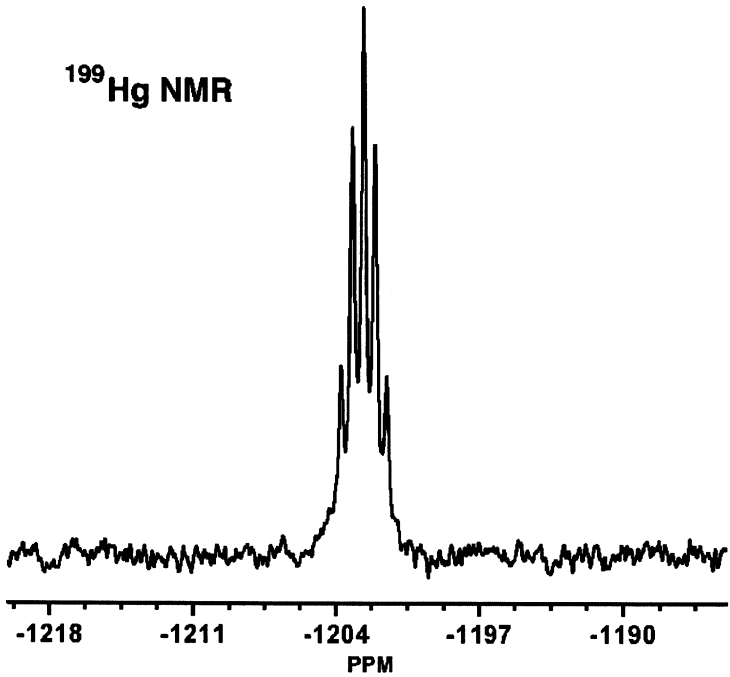

FIGURE 9 89.312 MHz ^{199}Hg $\{^1H\}$ NMR spectrum of $[Au_2Hg(P_2phen)_3](PF_6)_2$, **10**, in CD_3CN at 25°C demonstrating a single mercury environment coupled to six equivalent phosphorus nuclei.

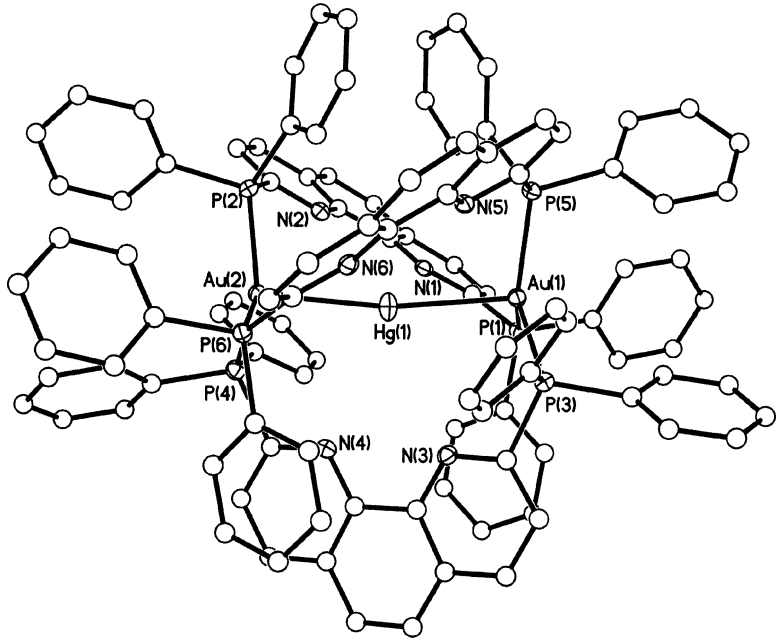

FIGURE 10 Crystal structural diagram of $[Au_2Hg(P_2phen)_3](PF_6)_2$, **10**, with carbon atoms drawn as open circles and thermal ellipsoids drawn at 40%. Selected distances (Å) and angles (°): Au(1)–Hg(1) 2.7847(4), Au(2)–Hg(1) 2.7807(4), Hg(1)–N(1) 3.589(2), Hg(1)–N(2) 3.636(2), Hg(1)–N(3) 3.374(2), Hg(1)–N(4) 3.378(2), Hg(1)–N(5) 3.659(2), Hg(1)–N(6) 3.604(2), Au(1)–Hg(1)–Au(2) 170.48(1), P(1)–Au(1)–P(3) 113.01(6), P(1)–Au(1)–P(5) 124.49(6), P(3)–Au(1)–P(5) 117.63(6), P(2)–Au(2)–P(4) 116.01(6), P(2)–Au(2)–P(6) 125.32(5), P(4)–Au(2)–P(6) 113.44(6), P(1)–Au(1)–Hg(1) 98.14(4), P(3)–Au(1)–Hg(1) 94.74(4), P(5)–Au(1)–Hg(1) 98.90(4), P(2)–Au(2)–Hg(1) 98.61(4), P(4)–Au(2)–Hg(1) 95.72(4), P(6)–Au(2)–Hg(1) 98.31(4).

which exhibits a single at 34.8 ppm with ^{199}Hg satellites ($^2J_{P\text{-}Hg} = 48$ Hz, ^{199}Hg is 16.8% abundant, $I = 1/2$) and a heptet at -143.7 ppm that integrates properly for two PF_6^- anions. Additionally, the $^{199}Hg\{^1H\}$ NMR spectrum (Figure 9) displays a septet at-1199.8 ppm ($^2J_{Hg\text{-}P} = 48$ Hz), indicating a single Hg environment coupled to six chemically equivalent phosphorus atoms. The phosphine environment in **10** is slightly more shielded than that observed in either $[Au_2Tl(P_2phen)_3](PF_6)_3$ or $[Au_2Na(P_2phen)_3](PF_6)_3$ which show resonances at 45.7 and 45.5. ppm, respectively. The structure of **10** (Fig. 10) is very similar to other metallocryptands and contains two trigonally-coordinated Au(I) centers capping a D_3 symmetric cage containing a Hg(0) atom. The two Au atoms are distorted from their respective trigonal

coordination planes towards the Hg atom by ca. 0.3 Å each, and the Hg-N separations range from 3.374(1) to 3.659(1) Å. The charge balance is verified by the presence of only two PF_6^- counterions. The Au(1)-Hg(1) and Au(2)-Hg(1) separations are short and nearly identical at 2.7847(4) and 2.7804(4) Å, respectively. Given the scarcity of legitimate Hg(0) coordination compounds, it is very difficult to put these separations in context; however, they are shorter than the sum of the respective covalent radii (Au = 1.34, Hg = 1.49 Å), indicating a significant attraction between these closed-shell metals.

The short Au-Hg separation measured in $[Au_2Hg(P_2phen)_3](PF_6)_2$ is very similar to the corresponding separation found in the isoelectronic $[Pd_2Pb]^{2+}$ species, indicating that similar forces might be responsible for maintaining these strong interactions. Table 1 shows the metal-metal separations of the aforementioned P_2phen-based metallocryptates measured by X-ray crystallography along with the predicted metal-metal separations calculated from the sum of covalent radii. The greatest attraction (or shortest separation) is observed in the Pd(0)-Pb(II)-Pd(0) system, where the resulting attractive ion-induced dipole interaction could stabilize this metal-metal interaction. Conversely, the longest metal-metal interaction (and perhaps, weakest) is observed in the Au(I)-Tl(I)-Au(I) species, where the added electrostatic repulsion of the like-charged metals negates much of the aurophilic attraction of the Tl(I) ion. As expected, decreasing the charge on the cation should weaken the dipole, and accordingly the monovalent Tl(I) ion is held less strongly than the isoelectronic, divalent Pb(II) ion in the Pd(0) and Pt(0)

TABLE 1 Intermetallic Separations and Angles of $[M_2M'(P_2phen)_3]^{n+}$ Metallocryptands

d^{10}Metal, M	Guest, M′	Separation, Å	M-M'-M angle, °	Ave. Δ d[a], Å	ref.
Pd(0)	Pb(II)	2.7095(6) 2.6902(6)	178.75(1)	−0.121	14
Pt(0)	Pb(II)	2.7469(6) 2.7325(6)	178.75(1)	−0.093	14
Pt(0)	Tl(I)	2.7907(9) 2.7919(9)	175.27(3)	−0.053	13
Pd(0)	Tl(I)	2.7914(6)	160.62(3)	−0.041	13
Au(I)	Hg(0)	2.7847(4) 2.7807(4)	170.48(1)	+0.007	16
Au(I)	Tl(I)	2.9171(5) 2.9109(5)	174.5(1)	+0.029	11

[a]Determined as the difference between the metal-metal separation as measured by X-ray crystallography and the predicted single-bond separation taken from a standard source.[17]

metallocryptands. The Au(I)-Hg(0)-Au(I) metallocrypate with the polarizable metal in the middle falls intermediate in this series. From this series it appears that simple ion-induced dipole interactions may play a significant role in stabilizing closed-shell metal-metal interactions. Along these lines the it was anticipated that a noble gas might be coaxed into the center of a Au-metallocryptand; however, the simple experiment of saturating a $-78°C$ chloroform solution of $[Au_2(P_2phen)_3](PF_6)_2$ (formed *in situ*) with $Xe_{(g)}$ did not show any encapsulation as probed by $^{31}P\{^1H\}$ NMR spectroscopy. Perhaps higher pressures may be necessary. Also, incorporation of trivalent lanthanide ions or Th(IV) into the Pd(0) or Pt(0) metallocryptands yielded equally disappointing results, suggesting the nature of the previously described metal-metal interactions may be more complicated than previously thought.

In a further attempt to explore the role of dispersion forces in maintaining short metal-metal separations, the encapsulation of Hg(0) by the zero-valent Pd_2- or Pt_2-based metallocryptand was explored. By eliminating the cationic charge, any attractive interaction would then be purely dispersive in nature, and the successful synthesis of Pt(0)-Hg(0)-Pt(0) or Pd(0)-Hg(0)-Pd(0) metallocryptands would provide an example of a purely metallophilic interaction. Unfortunately, the reaction of the appropriate Pd(0) or Pt(0) starting material with P_2phen in the presence of Hg(0) did not produce the anticipated zero-valent metallocryptands. Rather, serendipitous redox chemistry leads to the formation and encapsulation of a mercuros (Hg_2^{2+}) dimer (Scheme 4) that appears to be freely rotating within the cage at room temperature. The presence of two mercury atoms per cage is verified by the $^{31}P\{^1H\}$ NMR spectroscopy (Fig. 11), which shows ^{199}Hg satellities comprising ca. 34% of the total spectrum (^{199}Hg is 16.8% abundant, $I = 1/2$). The ^{199}Hg NMR for both **11** and **12** and the ^{195}Pt NMR spectra for **12** are complicated but consistent

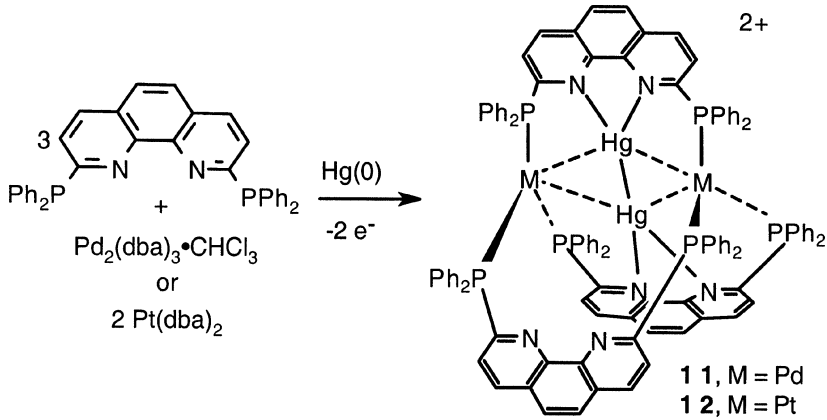

SCHEME 4

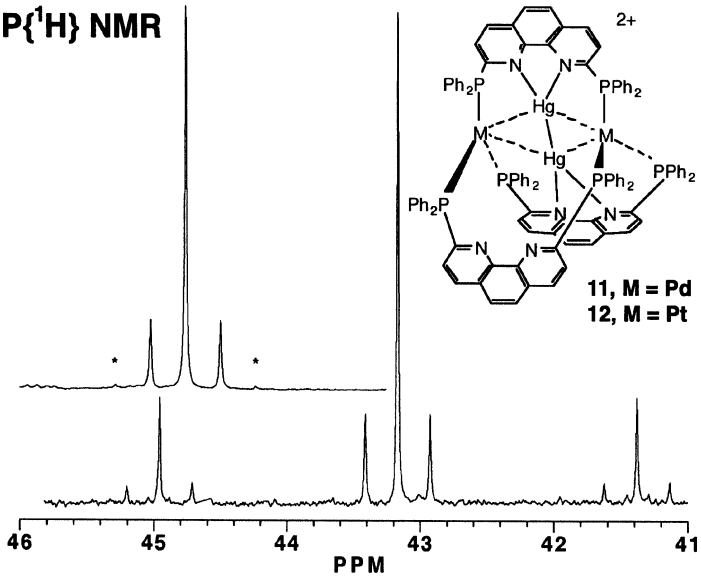

FIGURE 11 Downfield region of the 121.7 MHz $^{31}P\{^1H\}$ NMR spectra of **12** (upper left) in CD_3CN at 25°C showing coupling to ^{195}Pt (I = 1/2, 33.8% abundant) and ^{199}Hg (I = 1/2, 16.8% abundant) and of **11** (right) showing coupling to ^{199}Hg. Coupling to the isotopomer containing two ^{199}Hg atoms (triplet, 2.8% abundant) is denoted by the asterisks. A single phosphorus environment is observed down to −90°C suggesting a dynamic process involving the mercurous dimer.

with this formulation. Additionally, the single phosphorous environment at room temp. indicates that these two mercury atoms are dynamic. Reducing the temperature to −90°C does not stop this motion, and only slight broadening is oboserved. Metathesis to the BF_4^- of PF_6^- salts produces deep-red crystals identified by X-ray analysis to be $[Pd_2Hg_2(P_2phen)_3](BF_4)_2$, **11**, and $[Pt_2Hg_2(P_2phen)_3](PF_6)_2$, **12**.[18] These very similar structures (Fig. 12) are static in the solid state and have remarkably short metal-metal separations.

The Hg(1)-Hg(2) separation of 2.6881(4) and 2.7362(6) Å for **11** and **12**, respectively, are consistent with a formal metal-metal bond. The mercurous dimer interacts strongly and nearly symmetrically with the trigonally coordinated capping metals with Pt(1)-Hg(1), Pt(1)-Hg(2), Pt(2)-Hg(1) and Pt(2)-Hg(2), distances of 2.8045(5), 2.8258(6), 2.8447(6) and 2.7823(5) Å, respectively in **12**. In **11** the corresponding metrical parameters are very similar with Pd(1)-Hg(1), Pd(1)-Hg(2), Pd(2)-Hg(1) and Pd(2)-Hg(2) separations of 2.7936(6), 2.7475(5), 2.7419(5) and 2.7960(6) Å, respectively. The separations to the centroid of the Hg-Hg bond are even shorter (Fig. 13) with

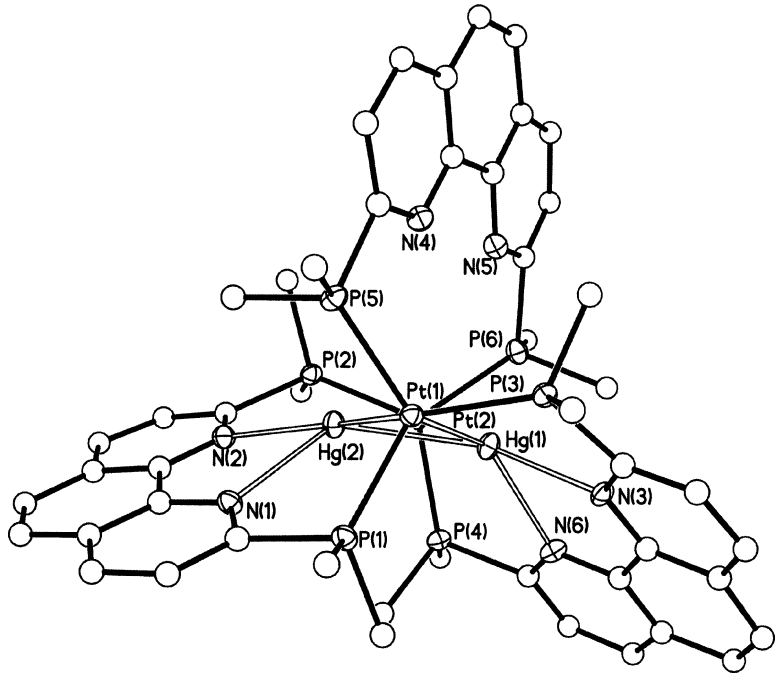

FIGURE 12 Thermal ellipsoid plot (40%) of cationic portion of $[Pt_2Hg_2(P_2phen)_3](PF_6)_2$, **12** with carbon atoms drawn as open circles and hydrogen atoms removed for clarity. All but the ipso carbon of the phenyl rings are removed for clarity. Distances (Å): Pt(1)–Hg(1) 2.8045(5), Pt(1)–Hg(2) 2.8258(6), Pt(2)–Hg(1) 2.8447(6), Pt(2)–Hg(2) 2.7823(5), Hg(1)–Hg(2) 2.7362(6), Pt(1)–P(1) 2.3017(17), Pt(1)–P(3) 2.2990(17), Pt(1)–P(5) 2.3246(18), Pt(2)–P(2) 2.3078(17), Pt(2)–P(4) 2.3175(17), Pt(2)–P(6) 2.3338(18), Hg(1)–N(1) 2.468(5), Hg(1)–N(2) 2.398(5), Hg(2)–N(3) 2.401(5), Hg(2)–N(4) 2.500(5), Pt···Pt 4.878(1), P(1)···P(2) 6.758(3), P(3)···P(4) 6.776(3), P(5)···P(6) 6.779(3). Angles (°): P(1)–Pt(1)–P(3) 120.20(6), P(1)–Pt(1)–P(5) 113.58(6), P(3)–Pt(1)–P(5) 108.84(6), P(2)–Pt(2)–P(4) 115.98(6), P(2)–Pt(2)–P(6) 115.26(6), P(4)–Pt(2)–P(6) 110.17(6), Pt(1)–Hg(1)–Hg(2) 61.313(15), Pt(1)–Hg(2)–Hg(1) 60.534(10), Hg(1)–Pt(1)–Hg(2) 58.152(13), Pt(2)–Hg(1)–Hg(2) 59.770(11), Pt(2)–Hg(2)–Hg(1) 62.052(13), Hg(1)–Pt(2)–Hg(2) 58.178(13), N(1)–Hg(1)–N(2) 67.44(19), N(3)–Hg(2)–N(4) 67.82(18), P(1)–Pt(1)–Pt(2)–P(2) 83.93(7), P(3)–Pt(1)–Pt(1)–Pt(2)–P(4) 88.77(6), P(5)–Pt(1)–Pt(2)–P(6) 88.98(7).

Hg_2(centroid)–Pt(1) and Hg_2(centroid)–Pt(2) separations of only 2.460 and 2.421 Å while in **11** the Hg_2(centroid)-Pd(1) and Hg_2(centroid)-Pd(2) distances are slightly shorter at 2.423 and 2.421 Å. It may be this interaction that leads to the dynamic behavior observed in solution. Interestingly, compared

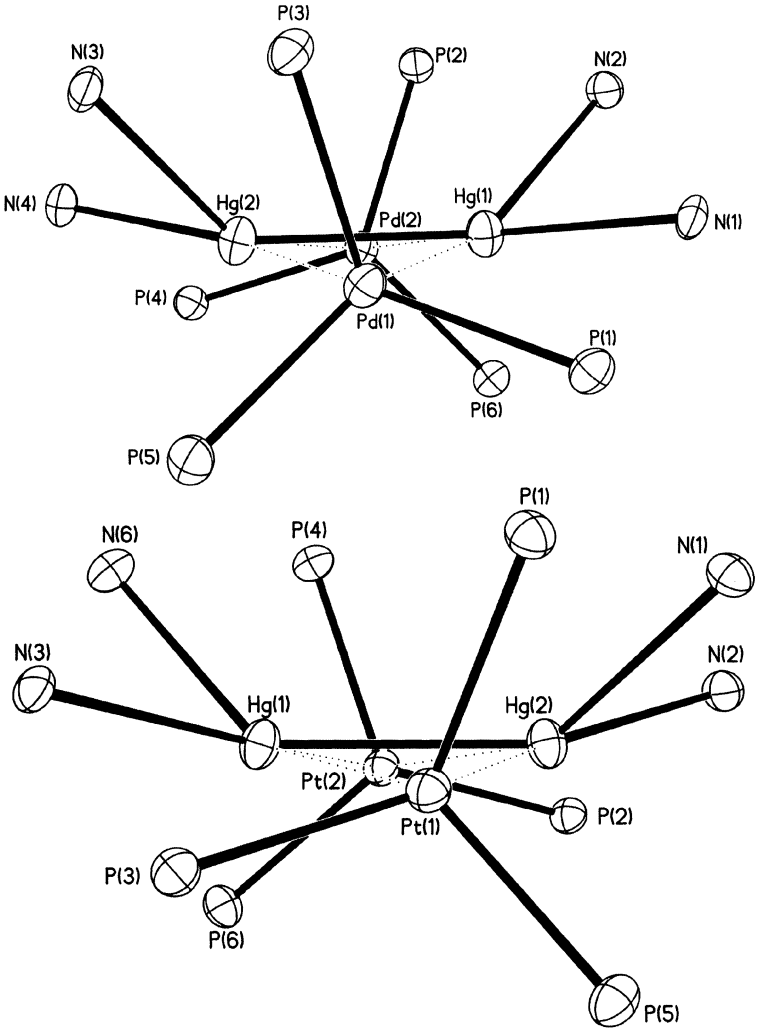

FIGURE 13 Comparison of the metal cores of **11** (top) and **12** (bottom). **12**: Hg(1)–Hg(2) 2.7362(6), Hg_2(centroid)–Pt(1) 2.460, Hg_2(centroid)–Pt(2) 2.459 Å. **11**: Hg(1)–Hg(2) 2.6881(4), Hg_2(centroid)–Pd(1) 2.423, Hg_2(centroid)–Pd(2) 2.421 Å.

to the other metallocryptands, the Hg–N separations here are very short with an average Hg–N separation of 2.442 Å in **12** and 2.410 Å in **11**, and in this light the dynamic behavior of the Hg_2^{2+} unit is even more striking.

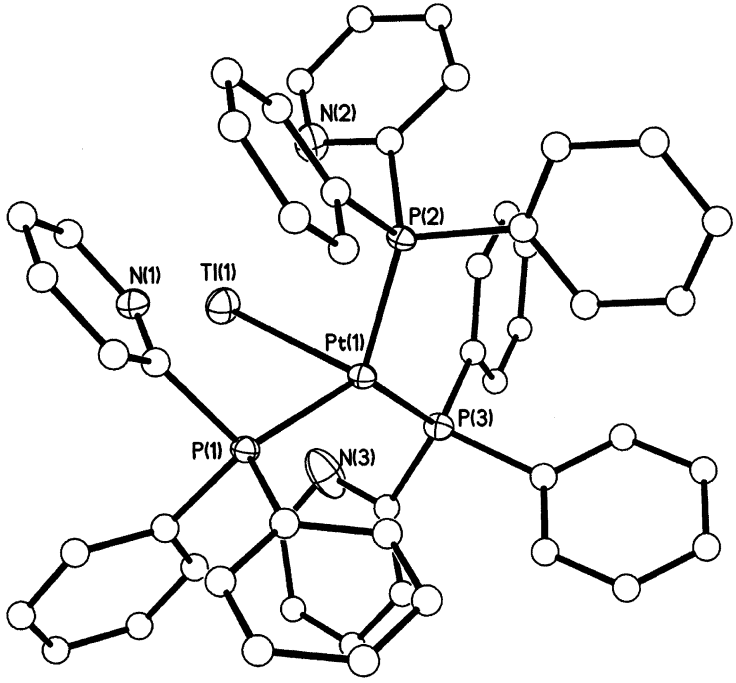

FIGURE 14 X-ray structural diagram of $[Pt(PPh_2py)_3Tl]NO_3$, **13** with hydrogen atoms removed for clarity and carbon atoms drawn as open circles. Selected bond lengths (Å) and angles (°): Pt(1)–Tl(1) 2.8888(5), Pt(1)–P(1) 2.297(2), Pt(1)–P(2) 2.280(2), Pt(1)–P(3) 2.281(2) P(1)–Pt(1)–P(2) 110.12(7), P(1)–Pt(1)-P(3) 129.15(7), P(2)–Pt(1)–P(3) 120.40(7), P(1)–Pt(1)–Tl(1) 86.18(5), P(2)–Pt(1)–Tl(1) 96.35(5), P(3)–Pt(1)–Tl(1) 93.50(5).

The short metal-metal separations observed in most of the complexes above are independent of any guest-ligand interactions, leading us to speculate whether the synthetically cumbersome P_2phen ligand was even necessary for producing these interactions. To probe these closed-shell metal-metal interactions in the absence of the metallocryptand cage the reactions between Tl^+ ion and the simple $(PR_3)_3Pt$ and $(PR_3)_3Pd$ compounds were probed. The anaerobic addition of a benzene solution of $Pt(PPh_2py)_3$ (PPh_2py = diphenyl-2-pyridylphosphine) to $TlNO_3$ produces an air-stable, red-orange solution from which very large crystals of $[Pt(PPh_2py)_3\ Tl]NO_3$, **13**,[19] could be isolated. The crystal structure (Fig. 14) shows a three-coordinate Pt(0) center witha a very short, unsupported Pt(1)-Tl(1) separation of 2.8888(5) Å. The pyridine ring does not appear to play a role in supporting the Tl^+ ion. In fact, a similar reaction is observed with $Pt(PPh_3)_3$ and Tl(I) ion a affording orange

solutions with unique ^{31}P and ^{195}Pt NMR spectroscopic chemical shifts, but X-ray quality crystals could not be grown. Substituting thallous nitrate for thallous acetate produces a similar product; however, the anion in this case coordinates to the Tl^+ ion producing $[Pt(PPh_2py)_3Tl]O_2CCH_3$, **14**.[19] Interestingly, in **14** the Tl^+ binding is dynamic at room temperature whereas in **13** the Pt-Tl interaction is maintained, suggesting that coordination to Tl influences that metal-metal bond. Like thier metallocryptand counterparts, no P-Tl coupling was observed for either of these solutions even though the interaction is maintained in solution.

Similiar interactions are observed with the analogous Pd(0) species, and $[Pd(PPh_2py)_3Tl]NO_3$, **15**,[20] was crystallized. This structure (Fig. 15) is isomorphous with its Pt analog, **13**, and also shows very short Pd-Tl separations of 2.858(1) Å. In all cases only the 1:1 salts formed, and there was no evidence for the formation of larger M(0)-Tl-M(0) complexes. More recently, we have extended these studies showing that similar interactions are observed with a variety of alkyl and aryl phosphines as well as Pb(II), Hg(II), Ag(I) and even Tl(III). The binding properties do not appear to follow

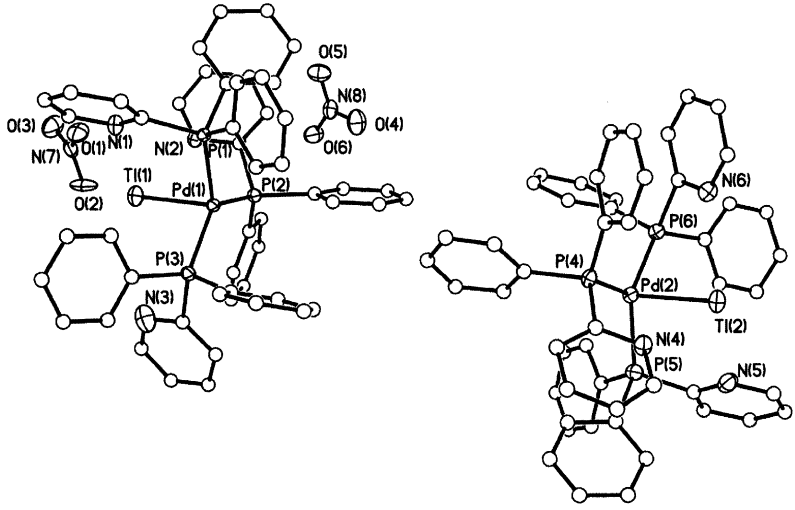

FIGURE 15 X-ray structural diagram of $[Pd(PPh_2py)_3Tl]NO_3$, **15** showing the asymmetric unit containing both Pd(0)–Tl(I) complexes and the nitrate counterions. The carbon atoms are drawn as open circle and hydrogen atoms are removed for clarity. Selected bond distances (Å) and angles (°) for Pd(1) containing species: Pd(1)–Tl(1) 2.8576(6), Pd(1)–P(1) 2.3219(16), Pd(1)–P(2) 2.3376(16), Pd(1)–P(3) 2.3219(16), P(1)–Pd(1)–P(2) 110.49(5), P(1)–Pd(1)–P(3) 119.98(6), P(2)–Pd(1)–P(3) 129.13(5), P(1)–Pd(1)–Tl(1) 95.97(4), P(2)–Pd(1)–Tl(1) 86.32(4), P(3)–Pd(1)–Tl(1) 94.20(4).

any trend based on phosphine basicity or electron configuration of the Lewis acidic metal. No binding was observed for alkali metals.

Besides the striking structural features in these complexes, the implications for catalysis are also significant. The role of Pt(0) and Pd(0) complexes in organic synthesis and catalysis is well known,[21] and it has been shown that *in-situ* addition of Tl(I) salts to some Pd(0) catalyzed reactions is an efficient method for controlling the regioselectivity and rate of catalysis.[22] These effects have often been attributed to Lewis acid interactions between the substrate and the cationic metal; however, our results suggest that metallophilic interactions between Pt(0) or Pd(0) and Lewis acids like Tl^{+} or Hg^{2+} in catalysis may be larger than previously thought. Given the huge numbers of easily accessible Pd(0)-phosphine complexes, a systematic study of these interactions and their ability to affect catalysis should be relatively simple and is clearly warranted.

The metallocryptands described above are capabe of binding a variety of metal ions and Hg(0); however, their utility would be greatly expanded if they are capable of binding anions. A simple modification to the ligand backbone allows this, and these altered metallocryptands can be used for encapsulation of halides. As depicted in Scheme 5, addition of aqueous HBr to P_2phen produces the yellow hydrobromide salt of the ligand, which can then be added to the colorless gold(I)-metallomacrocycle to produce the deep orange anion encapsulated metallocryptate, $[Au_2Br(HP_2Phen)(P_2\text{-}Phen)_2](PF_6)_2$, **16**.[23] The same methodology works for the incorporation of Cl- and I-, but X-ray quality crystals could only be obtained for the bromide salt. Figure 16 shows the X-ray structural diagram of **16**. The structure is very similar to the metal encapsulated structures, except this one contains a Br^{-} anion between the two AuP_3 units with Au(1)-Br(1) and Au(2)-Br(1) separations of 2.875(1) and 2.845(1) Å, respectively, and a Au(1)-Br(1)-Au(2) bond angle of 156.3(2)°. The hydrogen atom was not located in the

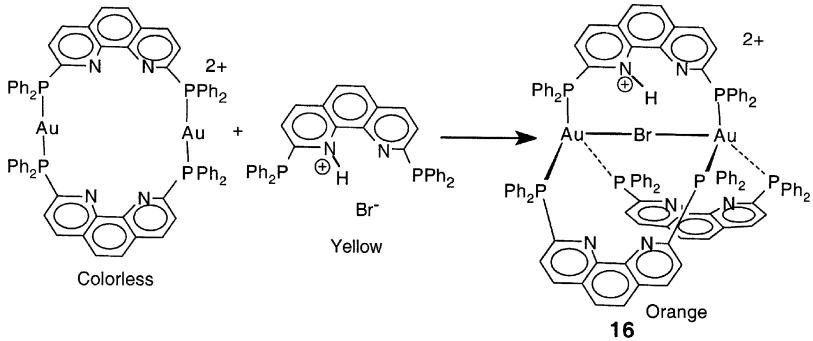

SCHEME 5

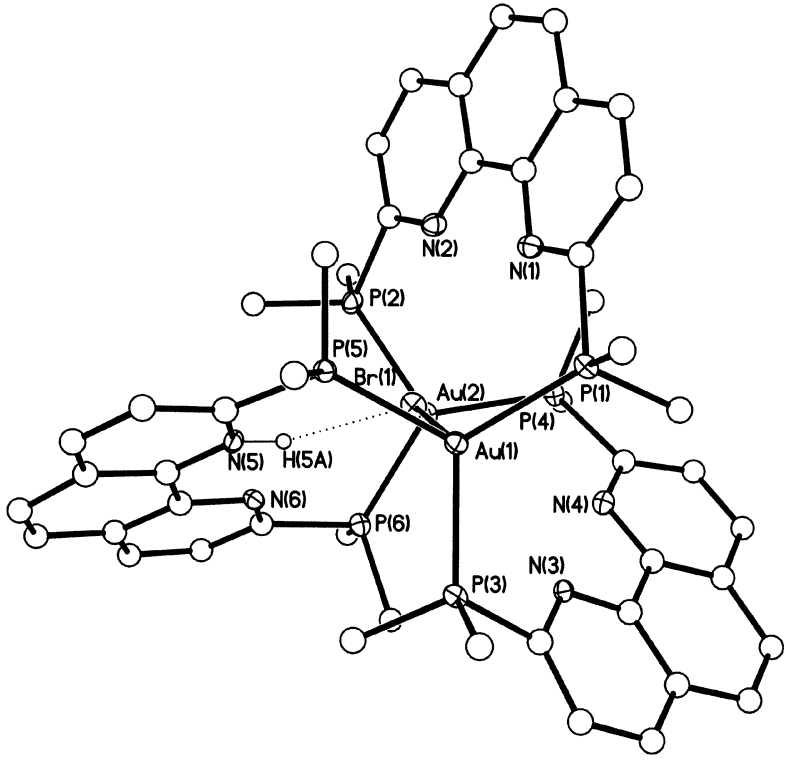

FIGURE 16 Structural drawing of the anion encapsulated Au(I)–metallocryptand. The hydrogen atom was not located and was placed on the nitrogen atom closet to the bromide ion. Selected bond distances (Å) and angles (°): Au(1)–Br(1) 2.8743(4), Au(2)–Br(1) 2.8450(4), Au(1)–Br(1)–Au(2) 156.39(2), Br(1)–N(5) 3.230, calee. Br(1)–H(5A) 2.301.

X-ray structure and was positioned on the N atom closest to the halide. The charge balance is verified by the presence of two PF_6^- counterions in the lattice. Attempts to exchange the encapsulated bromide for other halides or chalcogenides was unsuccessful as was the addition of tetrabutylammonium halide to the equilibrium mixture containing the empty metallocryptand described in eq. 2. Unlike the encapsulated mercurious dimer, the guest binding in **16** is not dynamic, and two sets of resonances are observed in the $^{31}P\{^1H\}$ NMR spectrum.

Thus far, the P_2phen ligand has been the most successful. Attempts to form metallocryptands with other ligands (Chart 1) have met with only limited success. Interestingly, in all of the reactions with P_2phen, no evidence of

polymer formation was observed, which is unusual given the propensity for multidentate ligands to form coordination polymers. The arrested polymer formation may be due in part to the orientation of the phosphorus lone pair, which are directed *inward* toward the imine groups, allowing for the structure to close onto itself, or it may be related to the observation that the rapid encapsulation appears to turn off ligand substitution at the d^{10} center. Conversely, as depicted in Scheme 6, reactions with 3,6-bis(diphenylphosphino)-pyridazine (P_2pz) and (tht)AuCl produce an interesting series of coordination polymers each with Au:ligand ratios of 2:3 and an empty metallocryptand capped by iodine atoms. Polymers **17** and **18**[24] can be interconverted by simple halide extraction or addition. Both of these can be converted into the empty, iodine-capped metallocryptand, complex $Au_2I_2(P_2pz)_3$, **20**,[24] (Fig. 17), which represents the first isolated empty cage. The Au···Au separation in $Au_2I_2(P_2pz)_3$ is very long at 7.373 Å, and attempts to incarcerate Na^+, Tl^+, Pb^{2+} or Hg(0) into this empty cage were unsuccessful. The lack of metal binding in **20** is not unexpected given the long Au-Au separation; however, it is possible to alter the cage size by metathesizing the iodine anions of other groups. For example, addition of NaSCN to a solution of **17** or **18** produces an unusual coordination polymer that contains chains of empty

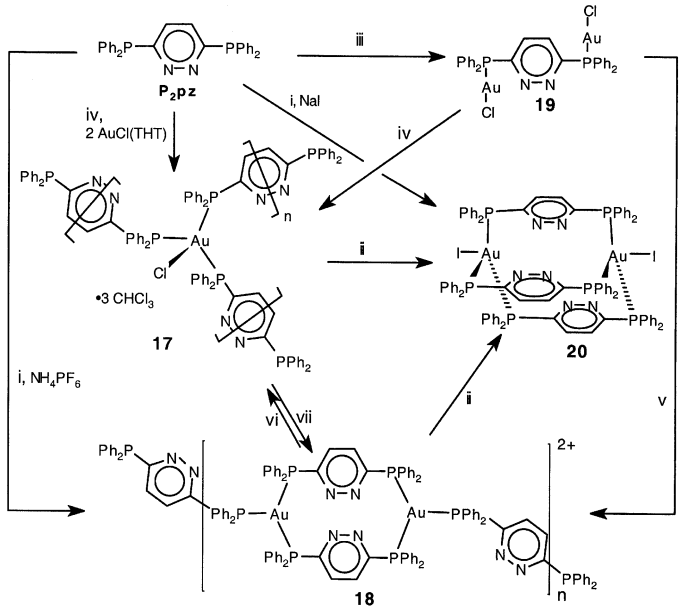

SCHEME 6

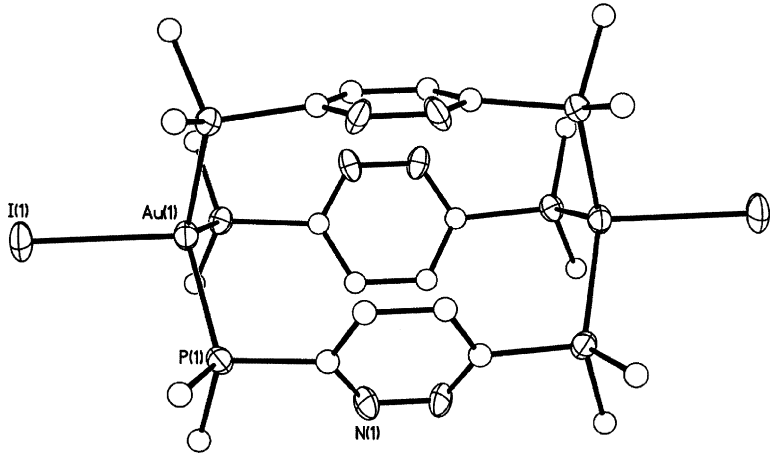

FIGURE 17 Thermal ellipsoid plot of $Au_2I_2(P_2pz)_3$, **20** with carbon atoms drawn as open circles. Hydrogen atoms and all but the ipso carbon of the phenyl rings removed for clarity. Selected bond distances (Å) and angles (°): Au(1)–P(1) 2.417(4), Au(1)–I(1) 2.8726(19), P(1)–C(1) 1.855(14), P(1)–C(3) 1.806(14), P(1)–C(9) 1.781(14), Au···Au 7.373, P(1)–Au(1)–I(1) 102.62(9).

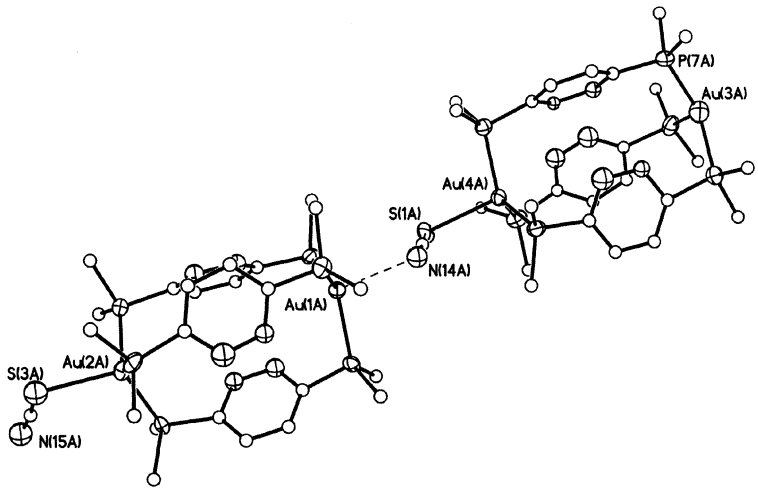

FIGURE 18 X-ray structural diagram showing two empty P_2pz based metallocryptands linked together by a SCN^- ligand. The Au···Au separation is 7.136 Å.

metallocryptands connected by bidentate SCN ligands (Fig. 18). The Au · · · Au separation shortens slightly to 7.136 Å. Conversion to the chloride species produces even greater distortions and several species were crystallized. Unfortunately, none of the structures refined satisfactorily.

Other ligands in Chart 1 were even less successful at producing cage complexes, even though their geometry is very close to that of P_2phen or P_2bpy. Attempts to produce mixed ligand species by adding one equivalent of a different ligand to $[Au_2(P_2phen)_2]^{2+}$ (formed according to Equation 2) only produced the disproportionated products.

CONCLUSIONS AND FUTURE OUTLOOK

Metallocryptands can be effective tools in probing metal-metal interactions, both in solution and in the solid state. The metal-metal separations described above are very short and in some cases shorter than the sum of the respective covalent radii, indicating a substantial attraction between these closed-shell heavy metal atoms or ions. The nature of this interaction is not well understood and continues to generate considerable theoretical effort, with most studies pointing to a combination of relativistic and/or correlation effects. Simplistically, we have demonstrated that simple ion-induced dipole interactions are good predictors of these attractive forces, and work is directed at using this notion to produce other multimetallic systems with similarly short separations.

By far the rigid P_2phen ligand has had the greatest success in forming cage complexes; however, its success does not preclude the use of other ligands even though we have had only limited success in their application. Given the cumbersome synthesis and air sensitivity of many phosphines, it would be advantageous to explore other classes of ligands that are capable of spanning two or more late metal ions. Recently, we developed a research program to employ the now ubiquitous N-heterocyclic carbene (NHC)

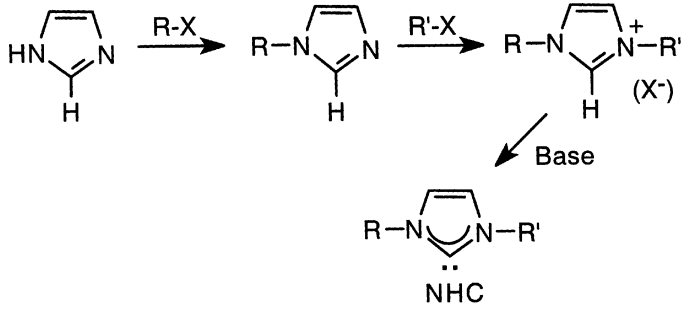

SCHEME 7

ligands[25,26] as supports for maintaining metal-metal interactions between closed-shell ions.[27] NHC ligands are considered better sigma donors than most phosphines,[28] significantly simpler to synthesize (Scheme 7), air-stable and although not realized with d^{10} ions, have the potential for metal-ligand back-bonding.[29] The challenge will be to develop synthetic in-roads into their Pt(0) and Pd(0) chemistry, which at this point, remains limited.

ACKNOWLEDGMENT

Acknowledgment is made to the National Science Foundation (CHE-0091180), to the Donors of the Petroleum Research Fund, administered by the American Chemical Society, for their generous financial support of this research. We are also indebted to Dr. Bruce C. Noll and Dr. Marilyn M. Olmstead for their expertise in obtaining and assisting with the X-ray crystallography, to Prof. John Nelson and Mr. Lewis Cary for their assistance with the multi-nuclear NMR Spectroscopy, and to Mr. John Vasquez for his contributions.

REFERENCES

1. Pyykkö, P. 1997. *Chem. Rev*. 97, 597–636.
2. Hamel, A., Mitzel, N. W., Schmidbaur, H. 2001. *J. Am. Chem. Soc*. 123, 5106. (b) Hayashi, A., Olmstead, M. M., Attar, S., Balch, A. L. 2002. *J. Am. Chem. Soc*. 124, 5791. (c) White-Morris, R. L., Stender, M., Tinti, D. S., Balch, A. L., Rios, D., Attar, S. 2003. *Inorg. Chem*. 42, 3237. (d) Fernández, E. J., Laguna, A., López-de-Luzuriaga, J. M., Monge, M., Pyykkö, P., Runeberg, N. 2002. *Eur. J. Inorg. Chem*. 3, 750. (e) Fernández, E. J., López-de-Luzuriaga, J. M., Monge, M., Olmos, M. E., Pérez, J., Laguna, A. 2002. *J. Am. Chem. Soc*. 124, 5942. (f) White-Morris, R. L. Olmstead, M. M., Balch, A. L. 2003. *J. Am. Chem. Soc*. 125, 1033. (g) Burini, A., Fackler Jr., J. P., Galassi, R., Grant, T. A., Omary, M. A., Rawashdeh-Omary, M. A., Pietroni, B. R., Staples, R. J. 2000. *J. Am. Chem. Soc*. 122, 11264.
3. (a) Pyykkö, P., Straka, M. 2000. *Phys. Chem. Chem. Phys*. 2, 2489. (b) Runeberg, N., Schütz, M., Werner, H.-J. 1999. *J. Chem. Phys*. 110, 7210.
4. (a) Pyykkö, P., Mendizabal, F. 1998. *Inorg. Chem*. 37, 3018. (b) Pyykkö, P., Mendizabal, F. 1997. *Chem. Eur. J*. 3, 1458. (c) Pyykkö, P., Runegerg, N., Mendizabal, F. 1997. *Chem. Eur. J*. 3, 1451.
5. Crespo, O., Fernández, E. J., Jones, P. G., Laguna, A., López-de-Luzuriaga, J. M., Mendía, A., Monge, M., Olmos, E. 1998. *Chem. Commun*. 2233.
6. Wang, S., Garzón, G., King, C., Wang, J.-C., Fackler, J. P., Jr. 1989. *Inorg. Chem*. 28, 4623.
7. Fernández, E. J., López-de-Luzuriaga, J. M., Monge, M., Olmos, M. E., Pérez, J., Laguna, A., Mohamed, A. A., Fackler, J. P., Jr. 2003. *J. Am. Chem. Soc*. 125, 2022.
8. Burini, A., Bravi, R., Fackler, J. P., Jr., Galassi, R., Grant, T. A., Omary, M. A., Pietroni, B. R., Staples, R. J. 2000. *Inorg. Chem*. 39, 3158.
9. Ziessel, R. 1989. *Tetrahedron Lett* 30, 463.
10. Catalano, V. J., Kar, H. M., Bennett, B. L. 2000. *Inorg. Chem*. 39, 121.

11. Catalano, V. J., Bennett, B. L., Kar, H. M., Noll, B. C. 1999. *J. Am. Chem. Soc*. 121, 10235.
12. Balch, A. L., Catalano, V. J. Chatfield, M. A., Nagle, J. K., Olmstead, M. M., Reedy, Jr., P. E. 1991. *J. Am. Chem. Soc*. 113, 1252.
13. Catalano, V. J., Bennett, B. L., Yson, R., Noll B. C. 2000. *J. Am. Chem. Soc*., 122, 10056.
14. Catalano, V. J., Bennett, B. L., Noll, B. C. 2000. *Chem. Commun.*, 1413.
15. (a) Crociani, B., Nicolini, M., Clemente, D. A., Bandoli, G. 1973. *J. Organomet. Chem*. 49, 249. (b) Carturan, G., Deganello, G., Boschi, T., Belluco, U. 1969. *J. Chem. Soc. A*, 1142.
16. Catalano, V. J., Malwitz, M. A., Noll B. C. 2001. *Chem. Commun.*, 581.
17. Pauling, L. 1967. *The Chemical Bond*, thaca, New York: Cornell University Press.
18. Catalano, V. J., Malwitz, M. A., Noll, B. C. 2002. *Inorg. Chem*. 41, 6553.
19. Catalano, V. J., Bennett, B. L., Muratidis, S., Noll, B. C. 2001. *J. Am. Chem. Soc*. 123, 173.
20. Catalano, V. J., Muratidis, S., unpublished results.
21. (a) Franks, R. J., Nicholas, K. M. 2000. *Organometallics*, 19, 1458. (b) Suginome, M., Nakamura, H., Matsuda, T., Ito, Y. 1998. *J. Am. Chem. Soc*. 120, 4248. (c) Tsuji, J. 1995, *Palladium Reagents and Catalysts*, New York: Wiley & Sons.
22. (a) Grigg, R., Loganathan, V., Santhakumar, V., Sridharan, V., Teasdale, A. 1991. *Tet. Lett*. 32, 687. (b) Grigg, R., Sridharan, V. 1993. *Tet. Lett*. 34, 7471. (c) Grigg, R., Kennewell, P., Teasdale, A. 1992. *Tet. Lett*. 33, 7789.
23. Catalano, V. J., Bennett, B. L., unpublished results.
24. Catalano, V. J., Malwitz, M. A., Horner, S. J., Vasquez, J. 2003. *Inorg. Chem*. 42, 2141.
25. Herrmann, W. A., Weskamp, T., Böhm, V. P. W. 2001. *Adv. Organomet. Chem*. 48, 1.
26. Herrmann, W. A., Köcher, C. 1997. *Angew. Chem., Int. Ed*. 36, 2162.
27. Catalano, V. J., Malwitz, M. A. 2003. *Inorg. Chem*. (in press).
28. Weskamp, T., Kohl, F. J., Hieringer, W., Gleich, D., Herrmann, W. A. 1999. *Angew. Chem., Int. Ed*. 38, 2416.
29. Green, J. C., Scurr, R. G., Arnold, P. L., Cloke, F. G. N. 1997. *Chem. Commun.*, 1963.